Applied Catalysis B: Environmental 142–143 (2013) 234–240

Contents lists available at SciVerse ScienceDirect

Applied Catalysis B: Environmental

journal homepage: www.elsevier.com/locate/apcatb

$AuCl_3$ on polypyrrole-modified carbon nanotubes as acetylene hydrochlorination catalysts

Xiaoyan Li [a,b], Mingyuan Zhu [a,b,*], Bin Dai [a,b,*]

[a] School of Chemistry and Chemical Engineering of Shihezi University, Shihezi, Xinjiang 832000, PR China
[b] Key Laboratory for Green Processing of Chemical Engineering of Xinjiang Bingtuan, Shihezi, Xinjiang 832000, PR China

ARTICLE INFO

Article history:
Received 5 January 2013
Received in revised form 14 May 2013
Accepted 16 May 2013
Available online 23 May 2013

Keywords:
Multiwall carbon nanotube
Gold catalysis
Polypyrrole
Acetylene hydrochlorination

ABSTRACT

In this study, polypyrrole (PPy) was deposited on the surface of multiwall carbon nanotubes (MWCNTs), and PPy–MWCNTs were used to support the $AuCl_3$ catalyst. Transmission electron microscopy and Fourier-transform infrared spectrometry confirmed the presence of PPy species in $AuCl_3$/PPy–MWCNT catalysts. $AuCl_3$/PPy–MWCNTs displayed enhanced catalytic activity and stability for acetylene hydrochlorination compared to $AuCl_3$/MWCNT. Electron transfer may occur between the N atom of PPy and the Au^{3+} center, which affects the adsorption of hydrogen chloride during acetylene hydrochlorination.

1. Introduction

Polyvinyl chloride is produced by the polymerization of vinyl chloride monomers (VCM), which are industrially manufactured by dichloroethane dehydrochlorination or acetylene hydrochlorination. Acetylene hydrochlorination is essential for VCM manufacturing in China because of China's vast domestic coal resources and the increasing cost of petroleum [1]. $HgCl_2$ supported on activated carbon is a common catalyst for industrial acetylene hydrochlorination. However, $HgCl_2$ complexes are toxic, and $HgCl_2$ can lead to serious environmental pollution problems. Therefore, non-mercury catalysts must be investigated as alternatives for acetylene hydrochlorination.

Several metal chlorides including Bi^{3+} [2], Pt^{6+} [3], Pt^{4+} [3,4] and Pd^{2+} [5] have been applied as possible non-mercury catalysts for acetylene hydrochlorination. Shen et al. [5] investigated the catalytic performance of $PdCl_2$ on activated carbon. The observed conversions of acetylene and selectivity for VCM were 98.70% and 97.95%, respectively. The catalytic activity of metal chlorides for acetylene hydrochlorination may be correlated with their standard reduction potential [6]. The standard electrode potential of Au^{3+} is 1.42 V, which is greater than that of Hg^{2+} (0.7961 V); thus, carbon-supported $AuCl_3$ catalysts display excellent catalytic performance for acetylene hydrochlorination [7,8]. Moreover, bimetallic catalysts composed of $AuCl_3$ and other metal chlorides exhibit improved catalytic performance during acetylene hydrochlorination. Shen et al. [9] synthesized a carbon-supported bimetallic Au–Cu catalyst. The obtained AuCu/C catalyst showed favorable catalytic activity and greater than 99.5% acetylene conversion and VCM selectivity. In our previous study [10], the addition of La^{3+} to an Au^{3+} catalyst reduced the amount of coke in the catalyst and inhibited the valence change of Au^{3+}. The conversion of acetylene was 98%, and the selectivity for VCM was greater than 99.8%. Although $AuCl_3$ and $AuCl_3$ derived bimetallic catalysts displayed favorable catalytic activity for acetylene hydrochlorination, they were easily deactivated as the reaction time on stream increased. Catalyst deactivation was attributed to the loss of Au^{3+} active species during acetylene hydrochlorination.

Several investigations have demonstrated the mechanisms by which Au^{3+} active species are lost during acetylene hydrochlorination. Hutchings et al. [11] proposed that acetylene is a better ligand than hydrogen chloride, which could be more easily adsorbed by $AuCl_3$ catalysts. Shen et al. [9] found that the initial coordination of hydrogen chloride with $AuCl_3$ produced a calculated energy of $-23.90\ kJ\ mol^{-1}$, whereas the presence of acetylene in the vacant co-ordination site of $AuCl_3$ generated a relative energy of $-66.65\ kJ\ mol^{-1}$. Therefore, the adsorption of acetylene on $AuCl_3$ is relatively stronger than that of hydrogen chloride. The electron in the *p* orbital of acetylene transfers to the unoccupied molecular orbital of Au^{3+}, which results in the reduction of Au^{3+} to its low valence state via the loss of Cl atoms [12]. Therefore, the stability of

* Corresponding authors at: School of Chemistry and Chemical Engineering of Shihezi University, Shihezi, Xinjiang 832000, PR China. Tel.: +86 993 2057270; fax: +86 993 2057210.
E-mail addresses: zhuminyuan@shzu.edu.cn (M. Zhu), db_tea@shzu.edu.cn (B. Dai).

0926-3373/$ – see front matter.
http://dx.doi.org/10.1016/j.apcatb.2013.05.031

$AuCl_3$ catalysts for acetylene hydrochlorination can be enhanced by inhibiting Au^{3+} reduction, which can be achieved by strengthening the adsorption of hydrogen chloride to the catalyst.

In the present study, we used N-doped multiwall carbon nanotubes (MWCNTs) to support $AuCl_3$ catalysts for acetylene hydrochlorination. A lone pair on the nitrogen atom of pyrrole was transferred to the Au^{3+} center via the interaction between the catalyst and support, which increased the electron density of the Au^{3+} center. $AuCl_3$ is the electron donor in the adsorption process of hydrogen chloride. Thus, an increase in the Au^{3+} electron density strengthened the bond between hydrogen chloride and $AuCl_3$. X-ray photoelectron spectroscopy (XPS) was used to identify the effects of the N-doped support and the electron state of Au^{3+}. The adsorption capacity of the catalysts was characterized by temperature-programmed decomposition (TPD). Transmission electron microscopy (TEM) images were used to monitor changes in the optical and morphological properties of the catalysts. Moreover, these catalysts were fully characterized by X-ray diffraction (XRD), temperature-programmed reduction (TPR), Brunauer–Emmett–Teller surface analysis (BET) and Fourier-transform infrared spectroscopy (FT-IR). A fixed-bed reactor was used to evaluate the catalytic performance of $AuCl_3$/MWCNT and $AuCl_3$/PPy–MWCNT catalysts.

2. Experimental

2.1. Materials

MWCNTs were purchased from Shenzhen Nanoport Company. $HAuCl_4{\cdot}4H_2O$ (with 47.8% Au content), C_2H_2 (gas, 98%), HCl (gas, 99%), and pyrrole (CP, >98%) were also used in the present study.

2.2. Catalyst preparation

Polypyrrole (PPy)-MWCNTs were prepared based on the process described in the literature [13,14]. A mixture of pristine MWCNTs (1.50 g), glacial acetic acid (0.45 mL) and distilled water (80 mL) was stirred for 30 min to obtain carbon slurry. Pyrrole (0.60 g), H_2O_2 (22.48 mL, 10%) and deionized water (20 mL) were added, and the solution was stirred for 24 h at room temperature in the dark. Finally, the solution was filtered and calcined at different temperatures under a nitrogen atmosphere for 4 h. The amount of pyrrole species was varied from 20 wt.% to 50 wt.%, and the obtained samples were labeled as 2PPy–MWCNT, 3PPy–MWCNT, 4PPy–MWCNT and 5PPy–MWCNT, respectively.

$AuCl_3$/PPy–MWCNT catalysts were prepared using an incipient wetness impregnation technique that employs aqua regia as a solvent, as described in the literature [15]. A solution of $HAuCl_4{\cdot}4H_2O$ (Strem, 31.98 mg) in aqua regia (3.19 mL) was added dropwise to the PPy–MWCNTs (1.50 g) while stirring for 1 h at room temperature. The PPy–MWCNTs were soaked for 24 h and were dried at 140 °C for 14 h. For comparison, the $AuCl_3$/MWCNT catalyst was also synthesized without pyrrole. The actual Au content of $AuCl_3$/2PPy–MWCNT, $AuCl_3$/3PPy–MWCNT, $AuCl_3$/4PPy–MWCNT, $AuCl_3$/5PPy–MWCNT and $AuCl_3$/MWCNT catalysts was 1.31 wt.%, 1.17 wt.%, 1.47 wt.%, 1.27 wt.% and 1.39 wt.%, respectively, as determined by inductively coupled plasma-atomic emission spectrometry.

2.3. Catalyst characterization

XRD data were collected using a Bruker D8 advanced X-ray diffractometer with Cu-K_α irradiation (λ = 1.5406 Å) at 40 kV and 40 mA in the 2θ scanning range of 10° and 90°. BET surface area analysis was performed by obtaining nitrogen adsorption isotherms at 77 K with a Micromeritics ASAP 2020 instrument. The morphologies of the samples were examined by TEM using a JEM 2010 electron microscope at an accelerating voltage of 200 kV, a line resolution of 0.14 nm and a point-to-point resolution of 0.23 nm. The FT-IR spectra were determined using a Nicolet Avatar 360 FT-IR spectrometer. TPD was performed using a Micromeritic ASAP 2720 instrument at a temperature ramp of 40–650 °C (ramp rate = 10 °C min^{-1}, flow = 45 mL min^{-1}, final temperature = 650 °C, hold time = 20 min). TPR was performed using a similar Micromeritic ASAP 2720 apparatus equipped with a TCD detector. The reducing gas was 10% H_2 in Ar, and the flow rate was 45 mL min^{-1}. The temperature was increased from room temperature to 650 °C at a heating rate of 10 °C min^{-1}. XPS data were recorded using an Axis Ultra spectrometer with a monochromatized Al-K_α X-ray source (225 W), a minimum energy resolution of 0.48 eV (Ag $3d_{5/2}$) and a minimum XPS analysis area of 15 μm.

The catalytic performance during acetylene hydrochlorination was evaluated in a fixed-bed glass microreactor (i.d. of 10 mm) operating just above atmospheric pressure. The temperature of the reactor was regulated by a CKW 1100 temperature controller (Chaoyang Automation Instrument Factory, Beijing, China). The reactor was purged with nitrogen to remove water and air in the reaction system before the reaction process. Hydrogen chloride gas was passed through the reactor at a flow rate of 20 mL min^{-1} to activate the catalyst. After the reactor was heated to 180 °C, acetylene (3.3 mL min^{-1}) and hydrogen chloride (3.8 mL min^{-1}) were fed through the heated reactor, which contained 2 mL of catalyst, at a gas hourly space velocity (GHSV) of 100 h^{-1}. The reaction products were analyzed by gas chromatography (GC-2014C).

3. Results and discussion

Representative TEM images of MWCNT, uncalcined 4PPy–MWCNT, pyrolyzed 4PPy–MWCNT and $AuCl_3$/4PPy–MWCNT catalysts are presented in Fig. 1. The tube thickness of MWCNT was 28.3 nm, as shown in Fig. 1a. The homogeneous dispersion of PPy on the outer surface of the MWCNT support was visible in the TEM micrographs. The thickness of the 4PPy–MWCNT tube reached 41.3 nm (Fig. 1b). Therefore, the PPy layer completely covered the MWCNT surface, which is consistent with the results described in the literature [14]. The black outer wall of the tube shown in Fig. 1c can be attributed to the carbonization of PPy at 800 °C. The $AuCl_3$/4PPy–MWCNT catalyst (Fig. 1d) exhibited a similar tube thickness as that of the corresponding 4PPy–MWCNT precursor. The TEM images confirmed the presence of PPy in $AuCl_3$/4PPy–MWCNT catalysts.

The FT-IR spectra of the MWCNTs, uncalcined 4PPy–MWCNT, pyrolyzed 4PPy–MWCNT and $AuCl_3$/4PPy–MWCNT catalysts are shown in Fig. 2. Compared to MWCNT, uncalcined 4PPy–MWCNT showed characteristic peaks at 1525, 1166, and 1032 cm^{-1}, which were assigned to the fundamental vibration of the PPy pyrrole ring, the C=C stretching vibration, and the =C—H in-plane vibration, respectively [16,17]. The FT-IR spectra of pyrolyzed 4PPy–MWCNT and $AuCl_3$/4PPy–MWCNT catalysts, which are shown in Fig. 2c and d, respectively, clearly displayed the same characteristic peaks as uncalcined 4PPy–MWCNT. Furthermore, the FT-IR results demonstrated that PPy existed on the MWCNT surface.

BET experiments were performed to investigate the changes in the MWCNT physical structure caused by the presence of PPy. The specific surface area and pore volumes of MWCNT, 2PPy–MWCNT, 3PPy–MWCNT, 4PPy–MWCNT and 5PPy–MWCNT carriers are summarized in Table 1. The surface area was determined by the BET method using nitrogen adsorption, whereas the pore volume was determined by mercury porosimetry. Compared to the MWCNTs, the BET surface area of PPy–MWCNT decreased from 89.11 m^2 g^{-1} to 79.70 m^2 g^{-1} as the pyrrole mass content increased from 20 wt.%

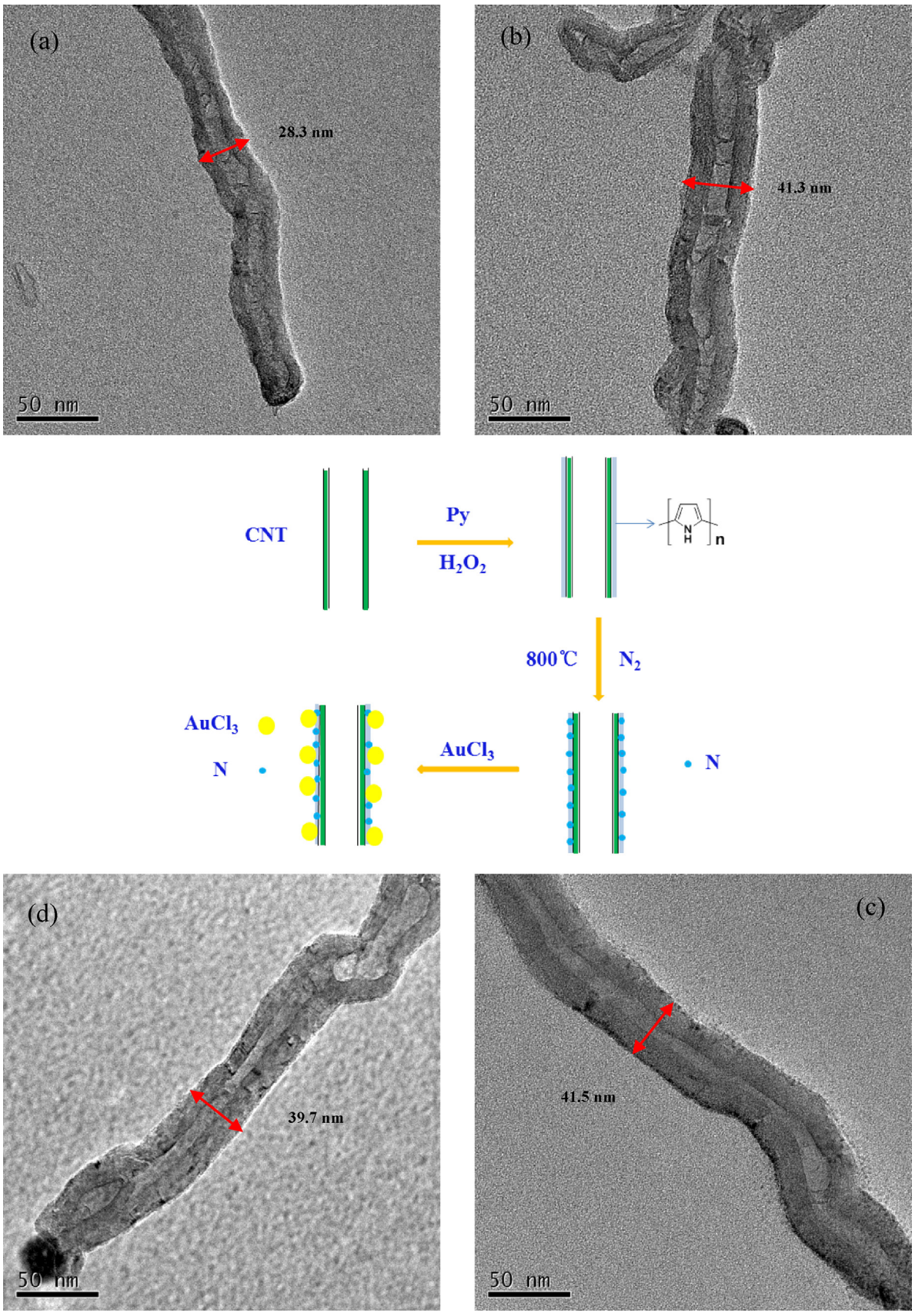

Fig. 1. TEM images of: (a) MWCNT, (b) uncalcined 4PPy–MWCNT, (c) pyrolyzed 4PPy–MWCNT and (d) $AuCl_3$/4PPy–MWCNT.

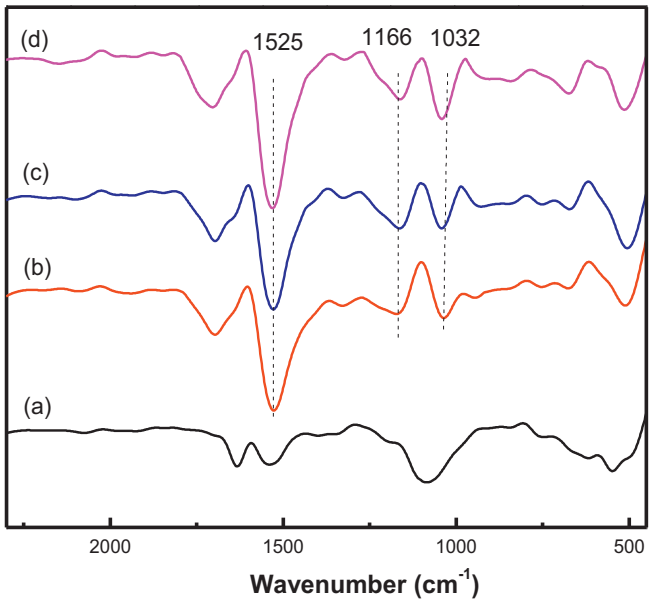

Fig. 2. FT-IR spectra of: (a) MWCNT, (b) uncalcined 4PPy–MWCNT, (c) pyrolyzed 4PPy–MWCNT and (d) $AuCl_3$/4PPy–MWCNT.

to 50 wt.%. This result suggested that PPy occupied part of the MWCNT pore space.

Catalysts with different MWCNT/PPy mass ratios of $AuCl_3$/PPy–MWCNT were compared to the $AuCl_3$/MWCNT catalyst under fixed reaction conditions (C_2H_2/HCl = 1:1.15, GHSV = 100 h^{-1}, reaction temperature = 180 °C) to verify the effect of additional PPy in $AuCl_3$ catalysts with respect to its catalytic performance during acetylene hydrochlorination. The reaction times for acetylene conversion of $AuCl_3$/MWCNT, $AuCl_3$/2PPy–MWCNT, $AuCl_3$/3PPy–MWCNT, $AuCl_3$/4PPy–MWCNT and $AuCl_3$/5PPy–MWCNT catalysts are illustrated in Fig. 3. The presence of PPy species promoted the initial catalytic activity of the $AuCl_3$/MWCNT catalyst and significantly enhanced the catalyst stability for acetylene hydrochlorination. The rate of acetylene conversion with the $AuCl_3$/MWCNT catalyst decreased from 40.22% to 34.02% after 10 h, indicating that the $AuCl_3$/MWCNT catalyst showed low activity under these reaction conditions. The $AuCl_3$/PPy–MWCNT catalyst displayed relatively higher catalytic activity than that of the $AuCl_3$/MWCNT catalyst. The amount of added PPy affected the catalyst stability. The $AuCl_3$/5PPy–MWCNT catalyst displayed optimal catalytic performance for acetylene hydrochlorination when the pyrrole mass content was 50 wt.%, as shown in Fig. 3. The increased activity of the $AuCl_3$/PPy–MWCNT catalyst was attributed to the presence of PPy species in the MWCNT, which changed the structure of the carbon nanotubes. To correlate the catalyst activity with the nitrogen content of the catalyst surface, XPS was systematically conducted to determine the nitrogen content of $AuCl_3$/MWCNT and $AuCl_3$/PPy–MWCNT catalysts. As shown in Table 2, the nitrogen content increased from 3.18 at.% to 3.88 at.% as the mass content of pyrrole increased from

Table 1
Textural parameters of the samples.

Samples	S_{BET} (m^2 g^{-1})	V (cm^3 g^{-1})	D (nm)
MWCNT	112.76	0.42	14.82
2PPy–MWCNT	89.11	0.31	14.00
3PPy–MWCNT	86.59	0.31	14.33
4PPy–MWCNT	85.24	0.31	14.60
5PPy–MWCNT	79.70	0.33	16.67

S_{BET}: surface area; V: total pore volume; D: average pore diameter.

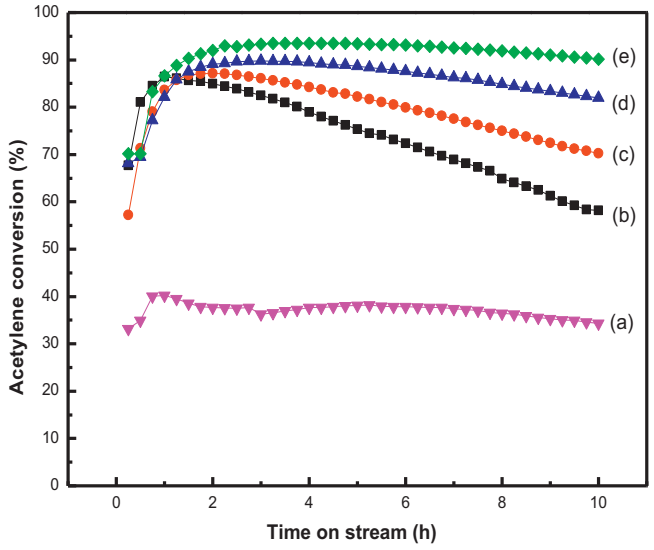

Fig. 3. Conversion of acetylene during acetylene hydrochlorination catalyzed by: (a) $AuCl_3$/MWCNT, (b) $AuCl_3$/2PPy–MWCNT, (c) $AuCl_3$/3PPy–MWCNT, (d) $AuCl_3$/4PPy–MWCNT and (e) $AuCl_3$/5PPy–MWCNT.

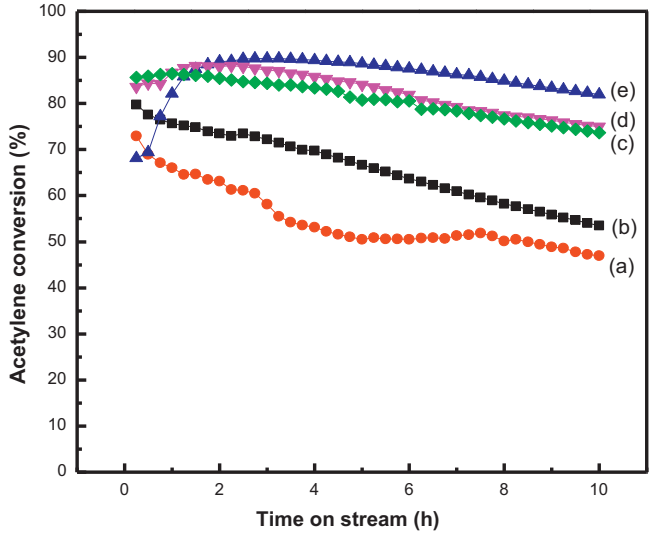

Fig. 4. Acetylene conversion of 4PPy–MWCNTs at different calcination temperatures: (a) 1000, (b) 900, (c) 600, (d) 700 and (e) 800 °C.

20 wt.% to 50 wt.%. This result demonstrated that an increase in the nitrogen content significantly enhanced the catalytic activity of $AuCl_3$/PPy–MWCNT.

In a further set of experiments, the 4PPy–MWCNT precursor was calcined in a tube furnace under a nitrogen atmosphere at 600, 700, 800, 900, and 1000 °C for 4 h. As shown in Fig. 4, the acetylene conversion and catalytic stability were both enhanced as the calcination temperature increased. The optimal reaction

Table 2
Surface atomic composition (%) of $AuCl_3$/MWCNT catalysts.

Catalyst treatment	Surface atomic composition (%)				
	Au 4*f*	N 1*s*	Cl 2*p*	O 1*s*	C 1*s*
$AuCl_3$/MWCNT	0.10		0.96	4.74	91.61
$AuCl_3$/2PPy–MWCNT	0.10	3.18	0.94	4.99	90.78
$AuCl_3$/3PPy–MWCNT	0.11	3.42	1.28	6.26	88.93
$AuCl_3$/4PPy–MWCNT	0.10	3.90	0.85	6.53	88.63
$AuCl_3$/5PPy–MWCNT	0.14	3.88	1.40	6.38	88.21

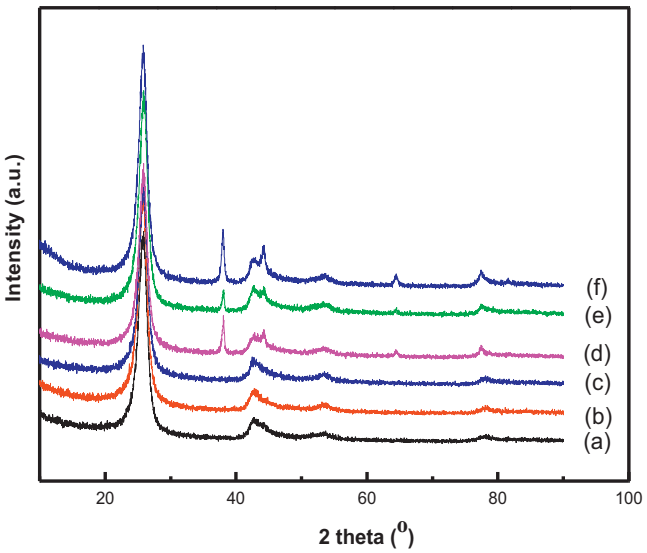

Fig. 5. XRD patterns of: (a) MWCNT, (b) 4PPy–MWCNT, (c) fresh $AuCl_3$/4PPy–MWCNT, (d) spent $AuCl_3$/4PPy–MWCNT, (e) fresh $AuCl_3$/MWCNT, and (f) spent $AuCl_3$/MWCNT.

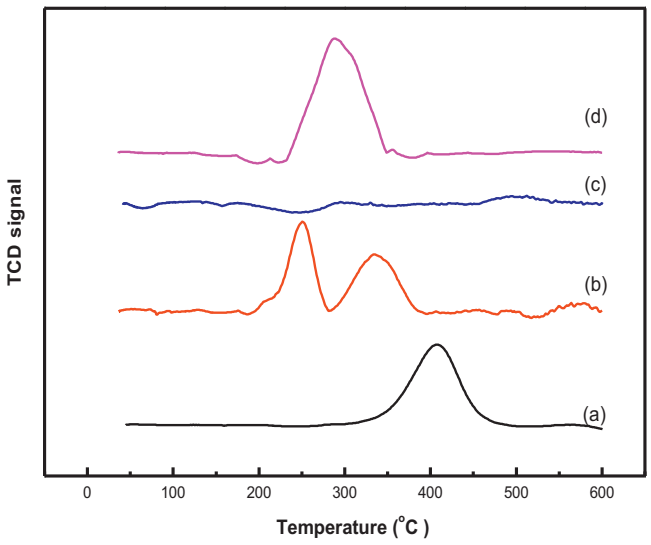

Fig. 6. TPR profiles of: (a) MWCNT, (b) fresh $AuCl_3$/MWCNT, (c) 4PPy–MWCNT and (d) fresh $AuCl_3$/4PPy–MWCNT.

conditions were obtained at a calcination temperature of 800 °C. However, temperatures greater than 800 °C caused catalyst deactivation, which implied that precursor calcination at extremely high temperatures may induce the decomposition of PPy species.

The XRD patterns of the carrier MWCNT, 4PPy–MWCNT, fresh $AuCl_3$/MWCNT, spent $AuCl_3$/MWCNT, fresh $AuCl_3$/4PPy–MWCNT, and spent $AuCl_3$/4PPy–MWCNT are shown in Fig. 5. Apart from the diffraction peaks of carbon nanotubes for fresh $AuCl_3$/MWCNT, several obvious diffraction peaks were observed in all of the samples at 38.12°, 44.34°, and 64.54°, corresponding to the (1 1 1), (2 0 0), and (2 2 0) planes of metallic Au^0, respectively [18]. However, the diffraction of Au^{3+} or metallic Au^0 was not observed in fresh $AuCl_3$/4PPy–MWCNT, indicating that active Au^{3+} components remained highly dispersed on the 4PPy–MWCNT support surface. This result showed that the presence of PPy in the $AuCl_3$/4PPy–MWCNT catalyst partly inhibited the reduction of Au^{3+} ions during acetylene hydrochlorination, which is consistent with the excellent catalytic activity and stability of the $AuCl_3$/4PPy–MWCNT catalyst. Spent $AuCl_3$/MWCNT and spent $AuCl_3$/4PPy–MWCNT clearly displayed the diffraction peaks of metallic Au^0, which showed that Au^{3+} was reduced to metallic Au^0 during acetylene hydrochlorination. The activity of Au-based catalysts for acetylene hydrochlorination can be ranked as follows: $Au^{3+} > Au^+ > Au^0$ [19,20]. Therefore, the reduction of Au^{3+} to metallic Au^0 is the main reason for the rapid deactivation of $AuCl_3$/MWCNT catalysts. However, it must be mentioned that the particle sizes of the spent $AuCl_3$/MWCNT and $AuCl_3$/4PPy–MWCNT catalysts are 18.9 nm and 17.7 nm, calculated by Scherrer formula. Agglomeration of Au particles occurs on both catalysts after acetylene hydrochlorination reaction. This results are opposite with the results of Hutchings et al., which reported that only a small amount of sintering of Au particles occurred in the process of acetylene hydrochlorination [11]. Therefore, the agglomeration of Au^0 particle may be another reason for the deactivation of Au-based catalyst in acetylene hydrochlorination, apart from the reduction of Au^{3+} to metallic Au^0.

TPR analysis provided further evidence that the addition of PPy to the $AuCl_3$/MWCNT catalyst inhibited changes in the valence of Au^{3+} during acetylene hydrochlorination. The TPR profiles for MWCNT, 4PPy–MWCNT, fresh $AuCl_3$/MWCNT and fresh $AuCl_3$/4PPy–MWCNT are shown in Fig. 6. The ca. 400 °C peak of the MWCNTs (Fig. 6a) was attributed to decarboxylation reactions and was assigned to oxygenated carbon functional groups on the carbon nanotube surface [20]. These peaks may be due to the oxidation of the carbon support by aqua regia. The reductive peak at approximately 228 °C was attributed to the reduction of Au^{3+} to Au^0 [15]. In contrast, the first reduction peak in fresh $AuCl_3$/MWCNT was observed at ca. 252 °C and was attributed to the reduction of Au^{3+}. The second peak at ca. 340 °C was attributed to decarboxylation. Compared to the original nanotubes, the forward migration of peaks may be due to the loading of the active ingredient. The sample of 4PPy–MWCNT (Fig. 6c) did not exhibit any peaks because the nature of the carbon nanotube surface was altered, which prevented the carboxylation of the nanotube surface by aqua regia. Bulushev et al. [21] demonstrated that $C{-}COOH + Au^{3+} \rightarrow C + Au^0 + H^+ + CO_2$ and proposed that Au^{3+} was reduced to Au^0 by carboxylic groups. 4PPy–MWCNT did not appear to decarboxylate the peaks, which indicated that the surface of the carboxyl groups on the carbon nanotube surfaces were suppressed by PPy. Thus, compared to MWCNT, only fresh $AuCl_3$/4PPy–MWCNT displayed an Au^{3+} peak. Therefore, the presence of PPy species inhibited the reduction of Au^{3+} to Au^0 during acetylene hydrochlorination.

The high-resolution spectra for the Au 4*f* orbital of $AuCl_3$/MWCNT and $AuCl_3$/4PPy–MWCNT catalysts and the N 1*s* orbital of the $AuCl_3$/4PPy–MWCNT catalyst are displayed in Fig. 7. The binding energies at 84.6 and 88.3 eV were attributed to the Au $4f_{7/2}$ and Au $4f_{5/2}$ spectra of metallic Au^0, respectively [22], whereas the spectra with binding energies at 86.2 and 89.9 eV were assigned to Au^{3+} [18]. The binding energy of the Au $4f_{7/2}$ of $AuCl_3$/4PPy–MWCNT catalyst showed a significant negative shift (~0.4 eV) compared to that of the $AuCl_3$/MWCNT catalyst. This negative shift was ascribed to the interaction between Au and PPy, which increased the electron density of Au^{3+} during electron transfer from N to the Au^{3+} center [23]. This phenomenon may be attributed to the compound structure formed by the N atoms of PPy and Au^{3+} via a π–σ coordination bond. The XPS spectra of nitrogen-doped MWCNTs in $AuCl_3$/4PPy–MWCNT are shown in Fig. 7b. Two different nitrogen states were observed for the $AuCl_3$/4PPy–MWCNT catalyst. The main peak at 400.4 eV was attributed to the formation of bonds between pyrrolic nitrogen bonds and hydrogen. The second peak at 398.8 eV may be derived from the pyridinic nitrogen on the edge of the graphene planes,

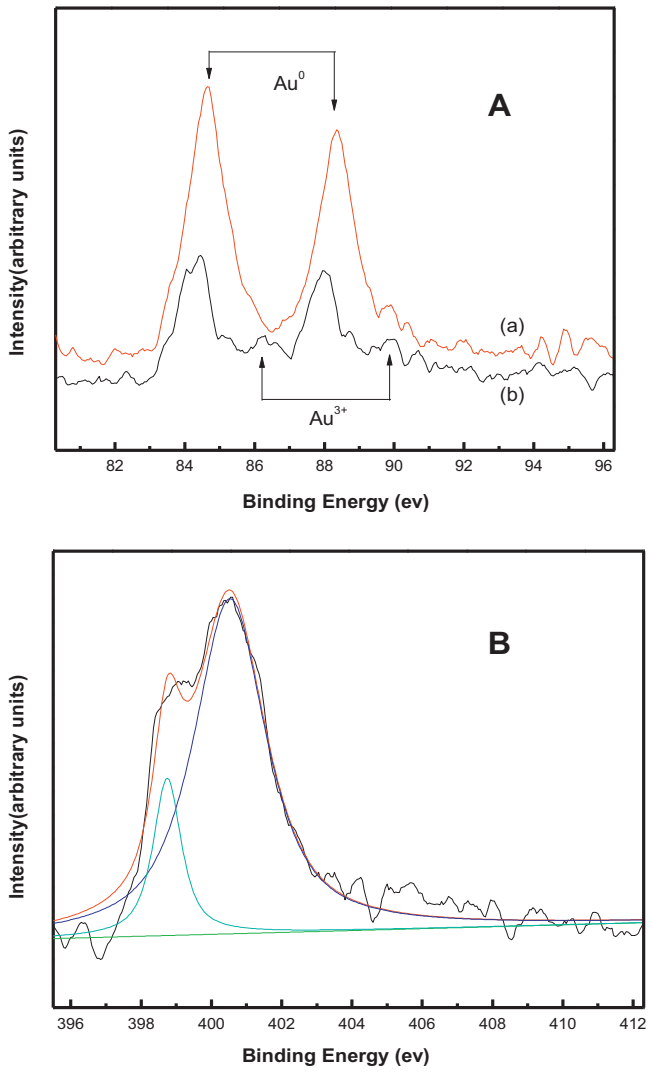

Fig. 7. High-resolution XPS spectra of: (A) the Au 4*f* orbital of (a) $AuCl_3$/MWCNT and (b) $AuCl_3$/4PPy–MWCNT and the (B) N 1*s* orbital of the $AuCl_3$/4PPy–MWCNT catalyst.

which was bonded to two carbon atoms in the graphene planes, donating one p electron to the aromatic π-system [14]. This result indicated that nitrogen π electrons, which could come from two nitrogen sources, were transferred to the empty orbital of gold, which enhanced the electron-donating ability of gold and allowed the catalyst to combine with more hydrogen chloride.

MWCNT and 4PPy–MWCNT lacked an adsorption peak for hydrogen chloride, as shown in Fig. 8. However, other data demonstrated the striking difference between $AuCl_3$/MWCNT and $AuCl_3$/4PPy–MWCNT catalysts during hydrogen chloride desorption. The fresh $AuCl_3$/MWCNT catalyst presented a band between 220 and 590 °C, which was characteristic of hydrogen chloride desorption. In contrast, the band representing hydrogen chloride desorption was absent in the TPD profile of $AuCl_3$/4PPy–MWCNT. Therefore, a large amount of hydrogen chloride was likely adsorbed by the $AuCl_3$/4PPy–MWCNT catalyst. The observed adsorption was caused by the interaction between PPy and $AuCl_3$, which changed the nature of the catalyst itself. This result was confirmed by XPS. Thus, the catalytic activity of TPD of $AuCl_3$/PPy–MWCNT increased during acetylene hydrochlorination.

To investigate the stability of the catalysts, we compared the stability of $AuCl_3$/MWCNT and $AuCl_3$/5PPy–MWCNT catalysts on stream 100 h, which is much longer than the 10 h run shown in

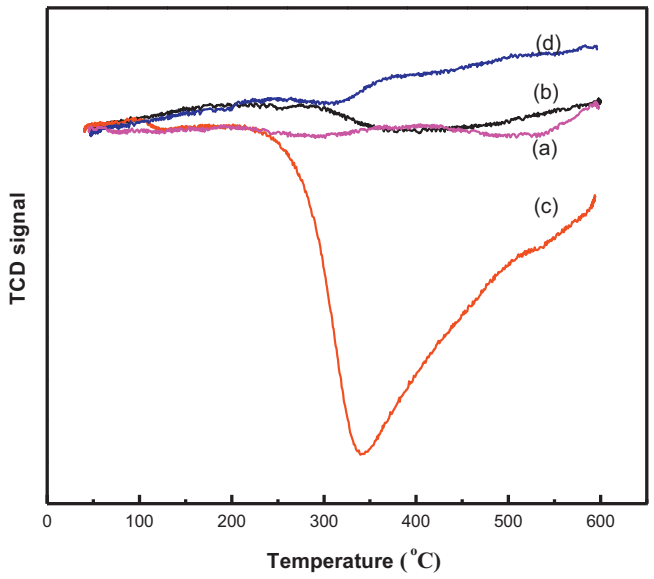

Fig. 8. TPD profile of: (a) MWCNT, (b) 4PPy–MWCNT, (c) fresh $AuCl_3$/MWCNT and (d) fresh $AuCl_3$/4PPy–MWCNT.

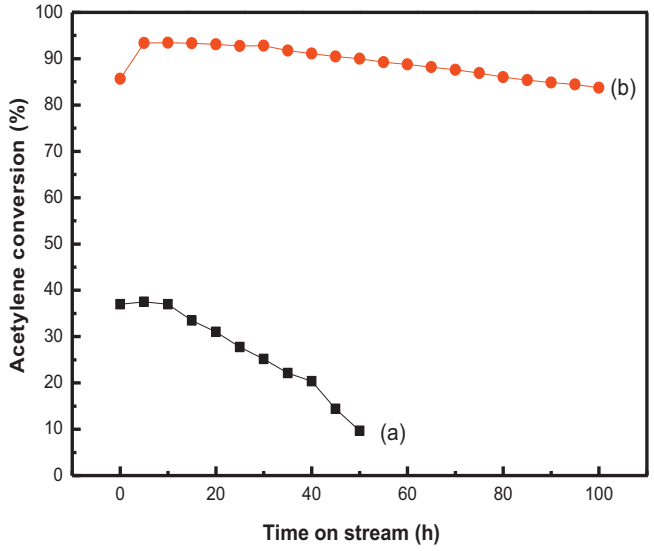

Fig. 9. Conversion of acetylene during acetylene hydrochlorination catalyzed by: (a) $AuCl_3$/MWCNT and (b) $AuCl_3$/5PPy–MWCNT.

Fig. 3. Fig. 9 clearly shows that the conversion of acetylene of $AuCl_3$/MWCNT decreased from 37.2% to 9.4% within 50 h, indicating its poor catalytic stability in acetylene hydrochlorination. However, the $AuCl_3$/5PPy–MWCNT catalyst displayed better catalytic activity and significantly enhanced stability, and its acetylene conversion only decreased by 10.3%, even after 100 h. This result demonstrated that the presence of a significant fraction of PPy species is essential for enhancing both the catalytic activity and stability of Au-based catalysts.

4. Conclusions

$AuCl_3$/PPy–MWCNT catalysts were prepared and used for acetylene hydrochlorination. $AuCl_3$/PPy–MWCNT displayed enhanced catalytic activity and stability during acetylene hydrochlorination compared to $AuCl_3$/MWCNT. The enhanced catalytic performance was attributed to electron transfer from PPy to the Au^{3+} center, which increased the adsorption of hydrogen chloride. The

excellent catalytic performance of the $AuCl_3$/PPy–MWCNT catalyst demonstrated its potential as an alternative to $HgC1_2$ catalysts for acetylene hydrochlorination.

Acknowledgments

This work was supported by the National Basic Research Program of China (973 Program, 2012CB720302), the Program for Changjiang Scholars and Innovative Research Teams in University (PCSIRT, IRT1161), and National Natural Science Funds of China (NSFC, U1203293).

References

[1] J.L. Zhang, N. Liu, W. Li, B. Dai, Frontiers of Chemical Science and Engineering 5 (2011) 514–520.
[2] D.M. Smith, P.M. Walsh, T.L. Slager, Journal of Catalysis 11 (1968) 113–130.
[3] S.A. Mitchenko, E.V. Khomutov, A. Shubin, Y.M. Shul'ga, Journal of Molecular Catalysis A: Chemical 212 (2004) 345–352.
[4] S.A. Mitchenkoa, T.V. Krasnyakova, R.S. Mitchenkoa, A.N. Korduband, Journal of Molecular Catalysis A: Chemical 275 (2007) 101–108.
[5] Q.L. Song, S.J. Wang, B.X. Shen, J.G. Zhao, Petroleum Science and Technology 28 (2010) 1825–1833.
[6] G.J. Hutchings, Journal of Catalysis 96 (1985) 292–295.
[7] B. Nkosi, N.J. Coville, G.J. Hutchings, Journal of Chemical Society, Chemical Communications 1 (1988) 71–72.
[8] B. Nkosi, N.J. Coville, G.J. Hutchings, Applied Catalysis 43 (1988) 33–39.
[9] S.J. Wang, B.X. Shen, Q. l. Song, Catalysis Letters 134 (2010) 102–109.
[10] H.Y. Zhang, B. Dai, X.G. Wang, L.L. Xu, M.Y. Zhu, Journal of Industrial and Engineering Chemistry 18 (2012) 49–54.
[11] M. Conte, A.F. Carley, C. Heirene, D.J. Willock, P. Johnston, A.A. Herzing, C.J. Kiely, G.J. Hutchings, Journal of Catalysis 250 (2007) 231–239.
[12] J.L. Zhang, Z.H.W.L. He, Y. Han, RSC Advances 2 (2012) 4814–4821.
[13] P.J. Wei, H. Tanabe, Carbon 49 (2011) 4877–4889.
[14] K.C. Lee, L.H.S.L. Zhang, R. Hui, Z. Shi, J.J. Zhang, Electrochimica Acta 54 (2009) 4704–4711.
[15] M. Conte, A.F. Carley, G. Attard, A.A. Herzing, C.J. Kiely, G.J. Hutchings, Journal of Catalysis 257 (2008) 190–198.
[16] L.H. Qiu, Y.J. Peng, B.Q. Liu, B.C. Lin, Y. Peng, M.J. Malik, F. Yan, Applied Catalysis A: General 230–237 (2012) 413–414.
[17] L.B. Sun, Y.C. Shi, L.Y. Chu, Y. Wang, L.Y. Zhang, J.R. Liu, Journal of Applied Polymer Science 123 (2012) 3270–3274.
[18] Y.W. Chen, H.J. Chen, D.S. Lee, Journal of Molecular Catalysis A: Chemical 363/364 (2012) 470–480.
[19] B. Nkosi, M.D. Adams, N.J. Coville, G.J. Hutchings, Journal of Catalysis 128 (1991) 378–386.
[20] M. Conte, C.J. Davies, D.J. Morgan, T.E. Davies, A.F. Carley, P. Johnston, G.J. Hutchings, Catalysis Science & Technology 3 (2013) 128–134.
[21] D.A. Bulushev, I. Yuranov, E.I. Suvorova, P.A. Buffat, L. Kiwi-Minsker, Journal of Catalysis 224 (2004) 8–17.
[22] X.Y. Liu, M.H. Liu, Y.C. Luo, C.Y. Mou, S.D. Lin, H.K. Cheng, J.M. Chen, J.F. Lee, T.S. Lin, Journal of the American Chemical Society 134 (2012) 10251–10258.
[23] A. Zwijnenburg, A. Goossens, W.G. Sloof, M.W.J. Craje, A.M. van der Kraan, L.J. Jongh, M. Makkee, J.A. Moulijn, Journal of Physical Chemistry B 106 (2002) 9853–9862.